The Response of Two Coupled 1-D Mixed Layer / Planktonic Ecosystem Models to Climate Change in the NE Subarctic Pacific Ocean

K.L. Denman[1] and M.A. Peña[2]

[1]Department of Fisheries and Oceans

Canadian Centre for Climate Modelling and Analysis

University of Victoria

P.O. Box 1700

Victoria, BC, Canada

V8W 2Y2

[2]Department of Fisheries and Oceans

Institute of Ocean Sciences

P.O. Box 6000

Sidney, BC, Canada

V8L 4B2

Submitted to *Deep-Sea Research II*, February 2001

Accepted, September 2001

Email: ken.denman@ec.gc.ca

Abstract

In this paper, we report on simulations of ecosystem responses to climate change with two planktonic ecosystem models, both coupled to a 1-dimensional mixed layer model run with annual wind and solar heating from Ocean Station P (50°N, 145°W) in the NE subarctic Pacific. The first ecosystem model is a four component model previously tested with extensive observations from OSP (Denman and Peña, 1999). The second ecosystem model is more complex, including phytoplankton partitioned into two size classes, and imposed grazing by mesozooplankton, which varies in time according to long term observations from OSP. Both models include temperature dependence of physiological rates. Two possible climate change scenarios are considered: (i) increasing ocean temperatures by 2°C (and 5°C) applied only to the ecological component, and (ii) changing the availability of iron to phytoplankton in the subarctic Pacific. Responses of the two models are similar, indicating that they are not primarily model dependent. In the warming cases, annual behavior and average standing stocks decrease marginally (≤10% for $\Delta T = 2°C$, and ≤22% for $\Delta T = 5°C$, second model only), ecosystem recycling increases with warming, and losses of organic particles to the ocean interior decrease (~10%) in the simpler model or increase slightly (<10%) in the complex model. Removal of any limitation by iron on phytoplankton growth changes phytoplankon standing stocks by 12% or less, but increases standing stocks of microzooplankton by 150% in the simple model and 225% in the complex model. The loss or export of organic particles to the ocean interior, indicative of the rate at which the ecosystem can sequester carbon, increases ~20% in the first model and 37% in the second model, all of the increase in the second model via grazing by the mesozooplankton. The winter-to-summer drawdown of surface layer nitrate increases in all the climate change simulations. Sensitivity of the second model for a warming of $\Delta T = 2°C$ to changes in the strength of temperature dependence of the physiological rates was generally small, except for changes in maximum microzooplankton biomass with increased dependence of their physiological rates. Increasing the temperature dependences of all physiological rates accentuated the vertical gradient in physiological rates resulting from the vertical temperature gradient, similar to what might be expected with increased thermal stratification.

1. Introduction

How marine planktonic ecosystems might respond to a changing climate is important to the carbon cycle because marine plankton affect the transformations and transport of carbon between the surface ocean and the ocean interior, thereby influencing atmospheric CO_2 concentrations. Primarily, the planktonic ecosystem transforms and partitions carbon into organic forms: (i) dissolved matter and suspended particles (roughly dissolved organic matter DOM) that are passively transported by ocean currents and mixing processes, and (ii) 'heavy' particles (roughly particulate organic matter POM) that can sink rapidly to the ocean interior. DOM and POM are continually being remineralized back to inorganic forms, primarily by bacteria, but at widely-varying rates. These ecosystem-induced transformations and partitioning of carbon into different forms vary geographically and temporally. Ecosystem models, to be applied to the cycling of carbon in the ocean, must be capable of predicting these geographic and temporal patterns.

Since the first efforts of Fasham et al. (1993) and Sarmiento et al. (1993) to couple an ecosystem model with an ocean general circulation model of the N. Atlantic, much progress has been made in the development of coupled models (e.g. Sarmiento et al., 1998; Oschlies and Garçon, 1999; Haigh et al, 2001). However, the many feedbacks in coupled models are sufficiently complex such that it becomes difficult to attribute whole model behaviour to specific processes, biological or physical, even in 1-dimensional models (e.g. Kawamiya et al., 1995; McClain et al., 1996; Denman and Peña, 1999, henceforth DP99; all for Ocean Station P). Additional complexities and challenges arise if these models are to be used to forecast potential future responses to perturbations resulting from human activities (e.g. Doney, 1999). For these reasons, it may be prudent first to explore and analyze the responses of planktonic ecosystem models to possible climate change scenarios, but coupled to a physical model that does not itself

respond to the climate change scenario, for example, by increasing upper ocean stability as the surface ocean warms. In this way, it should be possible to separate out the mechanisms of intrinsic ecosystem response to changing forcing from those that might result through response to changes in physical oceanographic processes.

In this paper we consider two possible climate change scenarios: an increased temperature and increased iron availability in a High Nutrient-Low Chlorophyll (HNLC) region. With regard to temperature, Laws et al. (2000) developed three predictors, including one based on solutions to a steady state ecosystem model, to analyze the main determinants on export production on global scales. They found that temperature alone can account for 86% of the variance over different regions of the 'ef ratio' = export production/total primary production. The other factor currently receiving much attention is the limitation on carbon uptake and hence on export of carbon by the micronutrient iron (e.g. Coale et al., 1996; Boyd et al., 2000), which has been implicated in glacial-interglacial differences in atmospheric CO_2 (e.g. Martin, 1990). Three areas where iron limitation has been demonstrated to be relevant are the HNLC regions: the Southern Ocean, the eastern Equatorial Pacific, and the NE subarctic Pacific.

To explore the potential responses of planktonic ecosystems to these climate change scenarios, we use a modification of a coupled mixed layer - ecosystem model that we developed for analysis of the ecosystem dynamics at Ocean Station P (50°N, 145°W) in the HNLC subarctic Pacific (DP99). To see whether the results we find are model-dependent, we develop in this paper a second ecosystem model, still coupled to the mixed layer model and driven with identical forcing. The modified model includes mesozooplankton, as prescribed grazing that varies over the year in proportion to the long term average annual cycle of mesozooplankton observed at OSP, and partitions the phytoplankton into two size classes to represent mainly pico-

and nanophytoplankton in the smaller size class and microphytoplankton in the larger size class. We analyze the results of these scenarios in terms of changes in standing stocks of phytoplankton and microzooplankton, in cycling within the ecosystem, in primary production, in export flux as a fraction of primary production, and in terms of winter-to-summer drawdown of surface layer nitrate.

2. The Mixed Layer Model

The one-dimensional mixed layer model, a Mellor-Yamada level 2.5 model (Mellor and Yamada, 1982) is the same model that we used in DP99 and is forced in an identical fashion, with annual cycles in winds and solar radiation characteristic of Ocean Station P (OSP), located at 50°N, 145°W in the northeast subarctic Pacific Ocean. The annual heat balance is balanced by a constant surface loss of heat from the sea surface, emulating approximately the long wave back radiation, and the model resolves the diurnal cycle (15 minute timestep). The mixed layer temperature (at midnight) varies annually between ~6 and ~13°C, close to the long term mean annual cycle observed at OSP (Whitney and Freeland, 1999). The model domain is 120 m deep divided into 60 two-m thick layers. The model employs an efficient implicit algorithm to mix temperature and salinity vertically each timestep, and the biological variables are mixed in the same manner. The bottom of the model domain corresponds to the permanent halocline which limits winter mixing in the NE subarctic Pacific.

Because the N.E. Pacific is an HNLC region, nitrate does not limit primary production. The source of new nitrate to the upper ocean (to replace the export flux over an annual cycle) is considered to be the upward flux of nitrate from Ekman upwelling (e.g. Gargett, 1991) into the subthermocline region above the permanent halocline, from where it is entrained into the surface layer each winter. In the model, nitrate is injected at a constant rate over the bottom 5 levels,

with the rate of nitrate injection set sufficiently high (in a preliminary run) in each simulation to maintain the ecosystem in a nitrate replete state. Although the export flux varies with time, the nitrate injected at a constant rate diffuses slowly upwards with time during most of the year, but then is entrained and mixed evenly throughout the water column when the mixed layer reaches the bottom of the model at the end of winter (see Denman and Peña, 1999 and Figure 5). Once the annual export flux is determined, the simulation is rerun with the injection rate set such that the annual injection of nitrate exactly matches the annual export flux, so that we could consider ecosystem behavior in an equilibrium annual cycle without the onset of nitrogen limitation. For the 'warming' scenarios, a constant offset (of 2° and 5°C) is applied to the initial temperature profile on 1 March: it affects the physiological rates in the ecological component, but has no effect on the mixed layer evolution, other than a constant temperature offset at all depths.

3. 'Mark 1' Ecological Model

3.1 Model description

The initial Mark 1 ecosystem model, described previously in DP99, consists of four components: dissolved inorganic nitrogen N, phytoplankton P, microzooplankton Z, and sinking organic particles D (see Appendix for equations). Iron limitation is formulated as a simple constant limiting factor on maximum phytoplankton growth. The version without temperature dependence of ecological rates has been evaluated against extensive observations from OSP. For this study, all growth, grazing and mortality rates are made temperature-dependent according to Q_{10} factors: e.g. for maximum phytoplankton growth rate n_m, at temperature $T+DT$,

$$n_m(T+\Delta T) = n_m(T) Q_{10}^{0.1\Delta T} \qquad (1)$$

The initial values for all rate parameters to which a Q_{10} temperature dependence is applied are referenced to a temperature of 10°C, since that is the approximate annual average temperature in the upper 50 m at OSP. That is, the values of these parameters given in Table 1 are for a temperature of 10°C: they vary with ambient temperature departures from 10°C according to eq. (1).

Q_{10}, the factor by which each physiological rate must be multiplied for an increase in temperature of 10°C, is set to 2 for phytoplankton (for n_m and m_{pd}), based on the work of Eppley (1972), primarily for diatoms. In the subarctic Pacific, Shiomoto et al. (1997) found that the rate of primary production by picoplankton (<2 μm) is also temperature dependent. Although other factors might limit the rate of *in situ* primary production, their two most statistically significant (linear) regressions give the rate of primary production (normalized to biomass) increasing by a factor of 1.4 and 2.1 for a 10°C warming, consistent with taking $Q_{10} = 2$. For all microzooplankton (and mesozooplankton, see Mark 2 model described later) rates (r_m, m_{zn} and m_{zd} for microzooplankton, and r_C for mesozooplankton), Q_{10} is set to 3, based on the synthesis of Huntley and Lopez (1992) for copepod growth. There is currently insufficient information to assign different Q_{10} values for micro- and mesozooplankton or for growth and loss rates. In the model, the action of bacteria is represented indirectly through the remineralization flux r_e. Although there is a broad range (at least 1 - 10) in the published literature for the temperature dependence of bacteria production, we set the Q_{10} for the remineralization rate to 3, near the midrange of recent estimates (e.g. White et al., 1991; Kirchman et al., 1993; Kirchman and Rich, 1997; Li, 1998).

The Q_{10} curves, such as those of Eppley (1972), are constructed from observations for many species, each representing the maximum instantaneous growth rate at its optimum temperature

(and light and nutrients). For phytoplankton and bacteria with high turnover rates, we might expect species selection in the marine environment to result in a species being dominant near its optimum temperature. A "community" maximum growth rate, which we implicitly assume in our model, should be lower at a given temperature, as the community includes species that are present but not near their optimum temperature. However, Banse (1995), who tabulated contemporary estimates of phytoplankton community growth rates "at ample irradiance", found many to approach the Eppley curve. In this model, we assume that while the maximum "community" growth rate will fall below the Eppley curve describing its temperature dependence, the shape of the temperature dependence can still be described by a Q_{10} as formulated in eq. (1). This species succession with changing temperature is least likely for mesozooplankton, where for some species there is only one generation per year.

For the 'standard' run, we use the same values for the model parameters as in the 'standard' run in DP99. The physiological rates (values given in Table 1 for a reference temperature of 10°C) now depend on temperature, but the annual cycles in the pool sizes remain basically unchanged from those in DP99, being slightly larger due to variation of the physiological rates with the annual cycle in temperature. As before, the annual cycle in *P* shows little variation (consistent with long term observations from OSP) except for a minor spring peak. The winter-summer drawdown in nitrate is 7.5 mmol-N m^{-3}, compared with the observed long term average ~7 mmol-N m^{-3} (Whitney and Freeland, 1999). The annual fluxes averaged over the top 50 m (Figure 1), are all within 10% of the original simulation except that the remineralization of detritus *D* back to the nutrient pool (the flux from *D* to *N*) has decreased by ~20%, because the rate of remineralization r_e below the mixed layer where temperatures are less than the reference

temperature 10°C has decreased. The ratio of export flux of *D* at a depth of 120 m to primary production (flux from *N* to *P*) is 0.22.

3.2 Climate change simulations with Mark 1 model

Two climate change simulations were performed with the Mark 1 model: a warming run with a 2°C temperature offset; and a run with iron limitation removed. In the simulation where iron limitation was removed, we increased the nitrate injection at the bottom of the model domain (simulating Ekman upwelling) from 0.20 to 0.37 mol-N m^{-2} y^{-1}, to maintain a repeating annual cycle in *N*. Otherwise, the model would eventually exhaust available nitrate, the supply of which may also be affected as the climate changes by physical processes not included in our study.

In the warming simulation (2°C offset), only small changes occur relative to the 'standard' run: mixed layer biomass of *P, Z* and *D* (at the time of maximum *Z*) change by less than 10%, recycling from detritus *D* to dissolved nutrient *N* increases by 29% because of the higher Q_{10} for bacterial remineralization, and export flux of *D* decreases by 15% (only % changes ≥ 15% are shown in Figure 2).

However, the simulation with increased iron availability produces significant changes (%-changes in Figure 2). In particular, primary production increases by 66%, *Z* by 150%, *D* by 119%, remineralization by 66%, and export flux by 29%. Although increases in the recycling fluxes back to the nutrient *N* match the increase in phytoplankton production, phytoplankton production and the recycling are largely out of phase, such that the drawdown of nutrient *N* (from winter maximum to summer minimum) increases by 78%. The annual cycle in mixed layer phytoplankton biomass remains unchanged while maximum biomass in zooplankton increases by 150%, a result also found in an earlier version of this model (Denman et al., 1998) with both linear and quadratic formulations of the mortality of the microzooplankton. Because model

behaviour and stability can depend on the formulation of mortality of the top predator (e.g. Edwards and Yool, 2000), we take the large increase in zooplankton biomass with both formulations to indicate that it may be a robust result of removing iron limitation, not an artifact of a particular model structure. The obvious question then is the following: Are these results robust to more significant changes in ecosystem model structure?

4. 'Mark 2' - An Enhanced Ecosystem Model

4.1 Model description

We made several enhancements to the Mark 1 model to create a Mark 2 ecosystem model. In the Mark 1 model, mortality of microzooplankton is used to 'close' the model; in the Mark 2 model, we extend the model to include the next higher trophic level, mesozooplankton. The Mark 1 model uses a linear mortality term to represent mainly grazing on microzooplankton by mesozooplankton, despite long term observations from OSP over the years 1956-80 (Fulton, 1983; Goldblatt et al., 1999) that document a large annual cycle in the abundance of mesozooplankton, presumably resulting in a large annual cycle in their food requirements. Hence, to represent time-dependent grazing on microzooplankton that is more consistent with observations, we first impose or specify a time-varying grazing by mesozooplankton (*Zo2*) proportional to the observed long-term annual cycle in mesozooplankton abundance. Second, since micro- and mesozooplankton graze on different size fractions of phytoplankton, we partition the phytoplankton population into a fraction <5μm (*Ph1*) representing pico- and nanophytoplankton, and a fraction >5μm (*Ph2*) representing microphytoplankton. Third, microzooplankton (now *Zo1*) are allowed to graze on detritus *D* (and indirectly on bacteria) and on small phytoplankton, and mesozooplankton graze on large phytoplankton and on

microzooplankton. All losses of mesozooplankton (except excretion) are assumed to sink out of the bottom of the model over an annual cycle without remineralization.

In this model, the phytoplankton are not divided into two separate compartments (or dependent variables, each with its own differential equation). Rather, grazing losses to microzooplankton and to mesozooplankton depend on the instantaneous partitioning between small and large phytoplankton. All phytoplankton are governed by the same nutrient, light and iron limitations on production rate and the same non-grazing mortality terms. The internal partitioning is based on observations that as the total chlorophyll increases, the proportion of small phytoplankton decreases (Søndergaard et al., 1991; Chisholm, 1992). In particular, Chisholm (1992) presented observations from the Mediterranean Sea (from Raimbault et al., 1988) showing that the small size fraction of phytoplankton (as chlorophyll biomass in <1, <3 and <10 μm size fractions) asymptotes to a constant concentration as the total chlorophyll concentration increases. This concept, that the small sizes of phytoplankton form a constant background in the ocean and that blooms consist primarily of larger diatoms being added to the background levels of pico- and nanoplankton forms the basis of a multiple food chain modelling approach of Armstrong (1994).

We have compiled recent observations of size fractions of chlorophyll from high latitude regions (Figure 3a). The studies from the North Atlantic (Joint et al., 1993; Savidge et al., 1995) reported fractions for depth-integrated biomass, as with some of the 'C-JGOFS-UBC' data (Boyd and Harrison, 1999); we divided all these values by the depth of integration. The rest of the observations are from the vicinity of OSP: the remaining 'C-JGOFS-UBC' data (http://www.meds-sdmm.dfo-mpo.gc.ca/jgofs/Default.htm) and the 'Peña' data were mixed layer averages or individual size fractions from below the mixed layer, and the 'Peña and Denman' data

were estimated from microscopic analyses to determine C:Chl ratios. In the model, we choose a rectangular hyperbola to describe the biomass of the small fraction *Ph1* as a function of the total phytoplankton biomass *P*:

$$Ph1 = \frac{P_S P}{k_S + P} \qquad (2)$$

where P_S is the asymptote of the small size fraction *Ph1* (taken as 2 mg-Chl m^{-3} in Figure 3), and k_S represents the value of *P* where *Ph1* is $0.5P_S$ (taken as 2.5 mg-Chl m^{-3} in Figure 3). One could argue for a different curve in Figure 3a (all the observations), but it is a reasonable representation of the observations only from the NE Pacific (shown in Figure 3b). The concentration of the large size fraction is just *Ph2 = P - Ph1*.

In this Mark 2 model, the microzooplankton can graze on both the small phytoplankton fraction *Ph1* and the detritus *D* (and indirectly on bacteria). We followed Fasham (1993) by setting the relative prey preference for *D* to be half that for *Ph1*. As in the various models of Fasham and coworkers, this preference results in *D* making up 15-20% of the diet of the microzooplankton. Various inverse analyses, models, and experimental results (Vézina and Platt, 1988; Fasham and Evans, 1995; Loukos et al., 1997; Rivkin et al., 1999) suggest that this proportion is too low, but Matear (1995) found that the pre-JGOFS data set from OSP was inadequate to constraint the preference parameters.

We have replaced the mortality term for microzooplankton with a time-varying grazing term that is proportional to the long term annual cycle in mesozooplankton biomass from OSP. Mesozooplankton composition data for OSP from R. Goldblatt and D. Mackas (personal communication) have been used to convert the mesozooplankton wet weight concentrations (Fulton, 1983; Goldblatt et al., 1999) to nitrogen units as follows: *Zo2* (mmol-N m^{-3}) = 1/14

(mmol-N m^{-3}/mg-N m^{-3}) x 1/12 (mg-N m^{-3}/ mg m^{-3}, dry weight) x 1/8 (mg m^{-3}, dry weight / mg m^{-3}, wet weight) = 7.4 x 10^{-4} *Zo2* (mg m^{-3}, wet weight).

The grazing is a Holling type III formulation with equal preference for micro-zooplankton *Zo1* and the large size fraction of phytoplankton *Ph2*:

$$\text{grazing by } Zo2 = r_C \cdot Zo2(t) \frac{(Ph2 + Zo1)^2}{k_Z{}^2 + (Ph2 + Zo1)^2} \qquad (3)$$

where *Zo2(t)* is the specified time varying concentration of mesozooplankton, r_C is the maximum grazing rate, and k_Z is the half saturation constant for the combined prey. The equations for the Mark 2 ecosystem model are included in the Appendix.

We carried out a number of sensitivity runs with the Mark 2 model to recover the typical conditions at OSP - a regular annual nitrate cycle in the surface layer between ~15 mmol-N m^{-3} in winter and ~ 7 mmol-N m^{-3} in summer, and a small seasonal cycle in phytoplankton biomass with an average concentration of 3-4 mmol-N m^{-3}. Parameter values for both versions of the model are shown in Table 1: changes to several parameters common to both models were required for the Mark 2 model to recover a reasonable annual cycle in the 'standard' run. However, the model structure has been changed significantly in the Mark 2 model: in particular the microzooplankton losses, m_{zn} + m_{zd} in the Mark 1 model, are now achieved mainly through time-dependent grazing by the mesozooplankton. Subsequently, when we tried to rerun the Mark 1 model with the parameter values from the 'standard' run of the Mark 2 model, the annual nitrate drawdown was only about 20%. This result is unrealistic given that the nitrate drawdown is about 50% based on long term observations, indicating that the two models cannot be made to behave similarly only by setting all common parameters equal in the two models.

Figure 4 shows a schematic of the Mark 2 model including annual mean fluxes for the upper 50 m of the water column, analogous to Figure 1 for the Mark 1 model. In the Mark 2 'standard' run, phytoplankton production and cycling around the foodweb are lower than in the Mark 1 standard run. The export flux of detritus *D* at a depth of 120 m (as a fraction of the primary production) is 0.17, compared with 0.22 for Mark 1. If the net flux of matter to the mesozooplankton *Zo2* is all assumed to exit the model to greater depths (due to sinking fecal pellets, sinking feeding debris, sinking or migrating animals) over the course of an annual cycle, then the export ratio *ER*, i.e. the total export flux *S* (0.38 mol-N m^{-2} y^{-1} which is 27% greater than that in the Mark 1 model) divided by the primary production *PP* (Table 2), increases to 0.43. The imposed grazing by mesozooplankton, varying over the year according to long term observations at OSP, thus represents a significant pathway of nitrogen (and presumed carbon) from the surface layer planktonic ecosystem.

The annual cycles for year 3 of the standard run in the Mark 2 model are shown in Figure 5. They show that an initial springtime increase in *P* seems to be triggered by the shoaling of the transient afternoon minimum mixed layer (top panel, red line), which occurs before the shoaling of the more well-defined nighttime maximum mixed layer depth. Also the bottom two time-depth sections for *P* and *D* show significant phytoplankton biomass produced in summer below the mixed layer, as well as the formation of detritus maxima below the mixed layer (and below the 50-m level used for the averages in Figures 4 and 6) following small peaks in mixed layer phytoplankton biomass concentration.

4.2 Climate change simulations with Mark 2 model

The two climate change scenarios, a 'global' warming offset of 2°C and removal of iron limitation on phytoplankton growth, were rerun with the Mark 2 modified ecosystem model.

However, current coupled climate models (e.g. Cox et al., 2000; IPCC, in press) are forecasting greater global warming over the next century, 4-5°C, rather than 2°C. Hence we have also considered the effect of a 5°C warming on the Mark 2 planktonic ecosystem model.

In the 2°C warming simulation, as with the Mark 1 ecosystem model, changes in the annual fluxes and standing stocks were small (%-changes ≥ 15% in parentheses in Figure 6a). The flux of *P* losses increased 15% to *D* and 26% to *Zo2* (a small flux), remineralization (flux from *D* to *N*) increased 29%, the same as for Mark 1, and excretion from *Zo2* to *N* increased 15%. Changes in export at 120 m were small and the increase in *Zo2* losses was offset by the reduction in export of sinking *D* due to increased recycling within the upper ocean ecosystem.

A 5°C warming causes a generally greater cycling around the ecosystem (Figure 6a, no parentheses), with the proviso that some of the original fluxes were small (Figure 4). The greatest increase (relative to the 'standard' run), 84% in the remineralization flux from *D* to *N*, results from a combination of increased fluxes to the detritus *D* and an increased remineralization rate. Although the losses via *Zo2* increased by 29%, this increase was matched by a decrease of 36% in the export of *D*, such that the total export increased only 4%, and the export ratio ER actually decreased to 0.34 (Table 2). As in the Mark 1 simulation of the removal of iron limitation (Fig. 2), the phytoplankton production is largely out of phase with the recycling back to *N*, such that the winter to summer drawdown of *N* increased by 27%. The peak concentrations of *P* and *Zo1* decreased by 15% and 22% respectively.

The removal of iron limitation has a profound effect on the maximum mixed layer standing stocks of microzooplankton *Zo1*, causing an increase of 225% (Figure 6b), with only minor changes in phytoplankton *P*, similar to the changes experienced in the Mark 1 model (Figure 2). The small change in the *P* cycle means that increased iron availability has not altered the relative

abundance of *Ph1* and *Ph2* in the model. Figure 7 shows that the increase in *Zo1*, relative to the standard run, is present throughout the year, not just during the summer maximum. Because the recycled fluxes now mostly follow the *Zo1* and *Zo2* pathways rather than via detritus, the time lag between the summer maximum in phytoplankton production and recycling back to *N* is smaller than in the Mark 1 model, such that the winter-to-summer drawdown of *N* increases only 40%, compared with 78% in the Mark 1 model. The large losses via the mesozooplankton *Zo2* more than counteract the reduced flux via *D*, such that the total export (*S* = sinking flux of *D* at 120m + *Zo2* losses except excretion) increases 37%, compared with 29% in the Mark 1 model. To balance the increased losses *S*, the injection of nitrate f_{up} had been increased from 0.38 (for the Mark 2 'standard' and warming runs) to 0.52 mol-N m^{-2} y^{-1}.

4.3 Sensitivity to changes in $\boldsymbol{Q_{10}}$

Given that published observations on Q_{10} values are sparce and span a large range, especially for bacteria, we investigated the sensitivity of the Mark 2 model to changes in the Q_{10} values, assuming first that they maintain their relative proportions, Q_{10}(phytoplankton): Q_{10}(bacteria): Q_{10}(zooplankton); and then to changes in the value of the Q_{10}, say for bacteria, while the values for phytoplankton and zooplankton are kept constant.

First, the $\Delta T = 2°C$ warming run for the Mark 2 model (Run 5, Table 2) was repeated with all three Q_{10} values adjusted together over a range of a factor of ten, in increments of roughly 50%. As with Run 5 (Fig. 6a), none of the maximum mixed layer poolsizes in *P*, *Zo1* or *D* changed by as much as 15% from Run 4. Variation in the annual primary production *PP* and export ratio *ER* = *S*/*PP* is shown in Figure 8a, normalized to the values in Run 5. For a factor of 10 change in the Q_{10} values, *PP* varied over a range of about 12%, and ER varied over a range of about 9%.

Second, varying the Q_{10}(zooplankton) over a factor of 10 caused the change (from Run 4) in maximum value in *Zo1* to vary from –29% to +17% (compared with a change of –10% in Run 5). Varation in annual mean *PP* and *ER* is shown in Figure 8b: neither flux changes by more than 3%.

Third, varying Q_{10}(bacteria) over a factor of 10 has little effect on the poolsizes or the fluxes (shown in Figure 8c): relative to Run 5, *PP* changes by about 2% and *ER* increases by about 10%. Since remineralization by bacteria should be increasing and hence increasing recycling, the increase of *ER* with increasing Q_{10}(bacteria) seems to be counterintuitive. However, the increasing *ER* is almost entirely due to an *increase* in the sinking flux of particles at 120 m while the sinking flux at 50 m remains roughly constant. The explanation appears to be that even with the 2°C warming, most of the water column below 50 m is still below the reference temperature of 10°C for the Q_{10}(bacteria), so the remineralization between depths of 50 and 120 m actually decreases as the Q_{10}(bacteria) increases. For a lower reference temperature or a larger warming offset (such that the temperature at all depths would be greater than the reference temperature 10°C), the remineralization below the summer mixed layer would increase with increasing Q_{10} but much less than above 50 m. Basically, increasing the Q_{10} values increases the vertical range in optimum physiological rates that results from the vertical temperature structure, but the specific results of this sensitivity analysis, i.e. the increasing *ER* in Figure 8c, should not be expected in all situations.

5. Discussion

5.1 Analysis of climate change simulations

Our main objective has been to consider potential effects of two climate change scenarios on the functioning of the subarctic Pacific planktonic ecosystem (as represented in our models)

isolated from the effects of changes in physical ocean conditions expected in response to climate change. All the climate change simulations with the Mark 1 and Mark 2 models, both increasing the temperature and removing the limitation of iron on phytoplankton production, result in increased phytoplankton production and increased recycling around the planktonic foodweb. The largest changes are the ~2-3 fold increase in microzooplankton populations for the simulations with increased iron availability (Figures 2 and 7). Unfortunately, because of methodological difficulties there are few observations of microzooplankton abundance and its variability with which to evaluate our model results.

Except for the 2°C warming simulation with the Mark 1 model, the climate change simulations result in increased total losses from the upper 120 m of the ocean (*S* in Table 2). However in all cases, the total losses decrease as a fraction of the primary production (*S /PP* in Table 2), confirming that recycling becomes relatively more important. The removal of iron limitation results in increased export losses, but recycling increases relatively more, even though there is no increase in the intrinsic biological rates, unlike in the warming cases.

The most likely physical changes to the ocean environment from a warming climate that we have not considered are gradual shoaling of the mixed layer and increased stability, both resulting primarily from freshening and warming of the surface ocean. Freeland et al. (1997) detected shoaling of the winter maximum mixed layer depth and a decrease of surface layer density in long term observations from OSP, and Whitney and Freeland (1999) detected an increase in stability near a depth of 100 m (their Fig. 9). We would expect these physical changes to affect phytoplankton production in two ways. First, shoaling of the mixed layer would result in increased average light levels for the phytoplankton in the mixed layer and probably increased primary production, since primary production is likely light-limited at OSP

for much of the year (Polovina et al., 1995; Harrison et al., 1999). Second, increased stratification would result in less nitrate (and iron) being transported up into the mixed layer from the ocean interior, with an eventual decrease in new production. Whitney and Freeland (1999) have observed reduced winter nitrate levels during the 1990s, extending out as far as OSP from the west coast of Canada. They showed the long term mean surface layer winter maximum nitrate at OSP to be ~16 mmol-N m^{-3} and the summer minimum to be ~9 mmol-N m^{-3}, for an average winter-to-summer drawdown of ~7 mmol-N m^{-3}. We have tuned the 'standard' runs for both Mark 1 and Mark 2 ecosysem models to have a drawdown of ~7.5 mmol-N m^{-3}, consistent with long term observations at OSP. In all the climate change simulations, we adjusted the 'upwelled' nitrate at the bottom of the model to match (approximately) the total export losses. From Table 2, the drawdown *DN* is 8.1-8.2 for the 2°C warming simulations, 9.5 for the 5°C warming, and 13.6 and 10.5 for the simulations with iron limitation removed. In all the perturbed cases, the annual drawdown is larger than the ~7 mmol-N m^{-3} from the long term observations at OSP. Thus, our climate change simulations indicate that nitrate available for phytoplankton during summer would likely decrease in the NE subarctic Pacific as the climate changes. However, changes in upper ocean nitrate distributions are not a good indicator of ecosystem change because they are strongly affected by physical processes as well, which, except for a warming offset, we have not considered here.

The analysis of sensitivity to changes in Q_{10} (Section 4.3) demonstrates a related effect of increased stratification: in the same way that increasing all the Q_{10} values increases the vertical range in optimum physiological rates because of the vertical temperature gradient, increasing the (thermal) stratification will increase the vertical range in optimum physiological rates such that with a more rapidly warming surface layer, cycling in the (warm) surface layer would speed up,

whereas cycling in (cooler) waters below the surface layer would either not increase or increase more slowly. Projecting changes in the export ratio *ER* would thus become more sensitive to the depth chosen for the calculation, i.e. *ER* might actually decrease at the base of the euphotic layer but increase if calculated at the depth of maximum winter mixing.

The increase in iron availability that we have simulated is an unlikely result of the warming expected over the next century. Rather, increased stability would likely decrease vertical mixing and hence decrease the supply of iron from below. However, in the subarctic Pacific, the main source of iron is believed to be aeolian deposition (Fung et al., 2000). Higher iron availability is usually associated with drier glacial periods; in fact, it was the analogy with glacial periods that led to the formulation of the iron limitation hypothesis to explain the existence of HNLC regions such as the NE subarctic Pacific Ocean (e.g. Martin, 1990). This hypothesis has led to several recent *in situ* iron fertilization experiments (e.g. Coale et al., 1996; Boyd et al., 2000), which have demonstrated iron limitation of phytoplankton growth. However, we cannot simulate these experiments with this model, because they have only observed the transient (~weeks) response, whereas our model addresses long term equilibrium changes in ocean conditions. We might indeed expect the expansion of HNLC regions with climatic warming (Fung et al., 2000), but other human activities leading to increased industrial activity, increased erosion, and changes in land use could increase the atmospheric iron supply to some oceanic regions that are now iron-limited (e.g. IPCC, 2001, chapter 3). Nevertheless, we need to understand mechanistically how marine ecosystems respond to changes in iron supply if we hope to forecast potential ecosystem responses to future changes in iron availability, both 'natural' changes associated with climate change and purposeful iron addition for enhancement of ecosystem production.

5.2 Future model requirements

The addition of mesozooplankton *Zo2* in the Mark 2 ecosystem model, even though specified as a time-varying grazing based on long term observations at OSP, rather than as a prognostic variable, significantly alters the internal dynamics of the ecosystem. Now a fraction of microzooplankton *Zo1* losses and detritus *D* (via *Zo1* grazing) flows to *Zo2*, where the portion not excreted back to *N* is lost through sinking fecal pellets, messy food particles, and sinking dead or migrating animals. From Table 2, *Zo2* losses are about 25% of primary production in the Mark 2 model, and are always greater than the export of *D* (i.e. greater than 50% of the total export *S*). This addition to the model of mesozooplankton required partitioning of phytoplankton into two size fractions, one prey for *Zo1* and the other prey for *Zo2*. Because most mesozooplankton progress through many developmental stages during the year, their role in cycling of nutrients and carbon may not be just proportional to their time-varying biomass; rather it may be necessary to consider changes in their functional role in the ecosystem as they progress through different developmental stages.

While we have partitioned phytoplankton into two size fractions according to the total biomass in the Mark 2 model, the functional dependence of primary production on light, nitrate and iron is the same for both fractions. Generally, large and small size classes of phytoplankton both appear to respond to iron addition, but the different observed responses may be a function of both iron dependence and grazing pressure (e.g. Cavender-Bares et al., 1999; Mann and Chisholm, 2000). In addition, diatioms have a greater silicon requirement. To address these issues, several studies have formulated models containing explicit phytoplankton size classes with different multiple nutrient dependencies for each size class (e.g. Fasham et al., 1999; Pondaven et al., 1999; Leonard et al, 1999; Chai et al., in press).

A primary role of the marine planktonic ecosystem in the ocean carbon cycle is to partition organic carbon into sinking POM and suspended DOM fractions, since POM is transported through gravitational sinking and DOM is transported through advection and diffusive mixing processes, which are dynamically distinct processes. Hence, in the future we also plan to partition detritus *D* into fractions that sink and are suspended, which we label for convenience as POM and DOM. Such an extended ecosystem model should be capable of partitioning carbon flow into POM and DOM in a manner that varies temporally and geographically, making it suitable to be coupled with a 3-dimensional ocean general circulation model.

6. Summary

We have simulated potential effects of climate change on two coupled models of the planktonic ecosystem and surface mixed layer. Our results can be summarized as follows:

- In global warming simulations with a 2°C offset, most rates and concentrations change by <10%, and there is generally greater recycling and less export of organic matter from the surface ocean. A 5°C warming, applied to the Mark 2 model, causes significantly greater ecosystem recycling, but little change in export to the ocean interior. For a 2°C warming, model sensitivity to expected ranges of uncertainty in the Q_{10} values is generally small, except for a significant range of variation in maximum microzooplankton biomass of 0.65 to 1.06 mmol-N m^{-3}, (representing a change from the control Run 4 of -29% to +17%) in response to a factor of 10 variation in Q_{10}(zooplankton).
- Removal of iron limitation can potentially increase annual primary production and maximum zooplankton standing stocks by more than a factor of 2, with little change to phytoplankton standing stocks, i.e. the increased primary production is passed on directly to the zooplankton. Although increased iron availability in the model causes export fluxes to

increase by 30-40%, the increased winter-to-summer drawdown of surface layer nitrate suggests that if long-term purposeful iron enhancement were implemented in the subarctic Pacific, macronutrient limitation would become prevalent, thus reducing the potential for increased export flux.

- The general results obtained with the Mark 1 model, increased recycling in all climate change runs and at least a doubling in mixed layer microzooplankton standing stocks in the runs with increased iron availability, are reproduced with the Mark 2 model, which includes imposed grazing by mesozooplankton, grazing on detritus/bacteria by micro-zooplankton, and size partitioning of phytoplankton. This lack of dependence on model structure argues for the robustness of these results.
- The similarity of the annual cycle of phytoplankton biomass in all these simulations suggests that satellite monitoring of phytoplankton biomass as an indicator of ecosystem responses to climate change may be difficult. Our results suggest that changes in primary production, rather than phytoplankton biomass, and changes in micro-zooplankton biomass may be more sensitive indicators of climate-induced change. However, the observational base for microzooplankton abundances cannot easily be improved without significant methodological development.

Appendix

The 'Mark 1' ecosystem model, developed in DP99, consists of four components: dissolved inorganic nitrogen *N*, phytoplankton *P*, microzooplankton *Z*, and sinking organic particles *D*, represented by the following set of four coupled ordinary differential equations:

$$\frac{dP}{dt} = (\text{growth})\ P - (\text{grazing})\ Z - m_{pd} P \qquad \text{(A1)}$$

$$\frac{dZ}{dt} = g_a(\text{grazing})\ Z - (m_{zn} + m_{zd})Z \tag{A2}$$

$$\frac{dN}{dt} = -(\text{growth})\ P + m_{zn}Z + r_e D + f_{up}(z_{\max}) \tag{A3}$$

$$\frac{dD}{dt} = (1 - g_a)(\text{grazing})\ Z + m_{pd}P + m_{zd}Z - r_e D + w_s \frac{dD}{dz} \tag{A4}$$

where

$$\text{growth} = v_m \ \text{Min}\left\{\left(\frac{N}{k_n + N}\right), \left(1 - \exp(-a\ I_{PAR}/v_m)\right), L_{Fe}\right\}, \text{ and} \tag{A5}$$

$$\text{grazing} = r_m \frac{P^2}{k_P^2 + P^2}. \tag{A6}$$

Under the assumption that only one factor limits phytoplankton growth at any time, the rate of phytoplankton growth is determined by the minimum value (evaluated each time step) of three functions, each ranging between 0 and 1, representing limitation by *N*, photosynthetically available radiation I_{PAR}, or iron Fe. I_{PAR} decreases with depth according to an exponential function, but with a absorption coefficient that depends on the vertical profile of 'biological particles': $k_t(z) = k_w + k_c(P(z)+D(z))$. The term f_{up} in (A3) represents the addition of nutrient at the bottom of the model at a constant rate to simulate average Ekman upwelling in the NE subarctic Pacific. All parameters are defined in Table 1, and are identical to those in DP99 except that now the physiological rates are temperature dependent according to the Q_{10} factors as defined in eq. (1): n_m and m_{pd} for phytoplankton; r_m, m_{zn} and m_{zd} for microzooplankton; and r_e, the remineralization rate representing indirectly the action of bacteria, all vary in time according to ambient temperature.

The 'Mark 2' ecosystem model consists of four dependent components: dissolved inorganic nitrogen *N*, phytoplankton *P*, microzooplankton *Zo1*, and sinking organic particles *D*. In

addition, phytoplankton *P* is partitioned into *Ph1*, small organisms less than 5 μm in size, and *Ph2*, larger organisms greater than 5 μm, according to the relation:

$$Ph1 = \frac{P_S P}{k_S + P}$$

where the parameters P_S and k_S are defined in Table 1. The mortality of microzooplankton *Zo1* and the large phytoplankton *Ph2* is now a function of a specified time-dependent concentration of mesozooplankton *Zo2*(t), with parameters defined in Table 1.

The set of coupled ordinary differential equations for the 'Mark 2' ecosystem model becomes:

$$\frac{\mathrm{d}P}{\mathrm{d}t} = (\text{growth})\ P - (\text{grazing1})\ Zo1\frac{Ph1}{Ph1 + p_D D} - (\text{grazing2})\frac{Ph2}{Ph2 + Zo1}Zo2(t) - m_{pd}P \qquad \text{(A7)}$$

$$\frac{\mathrm{d}Zo1}{\mathrm{d}t} = g_a(\text{grazing1})\ Zo1 - (\text{grazing2})\frac{Zo1}{Ph2 + Zo1}Zo2(t) - m_{zn}Zo1 \qquad \text{(A8)}$$

$$\frac{\mathrm{d}N}{\mathrm{d}t} = -(\text{growth})\ P + m_{zn}Zo1 + m_{cn}(\text{grazing2})\,Zo2(t) + r_e D + f_{up}(z_{\max}) \qquad \text{(A9)}$$

$$\frac{\mathrm{d}D}{\mathrm{d}t} = m_{pd}P + (1 - g_a)(\text{grazing1})\ Zo1 - (\text{grazing1})\frac{p_D D}{Ph1 + p_D D}Zo1 - r_e D + w_s\frac{\mathrm{d}D}{\mathrm{d}z} \qquad \text{(A10)}$$

where (*growth*) is given by eq. (A5) as before,

$$\text{grazing1} = r_m\frac{(Ph1 + p_D D)^2}{k_P^2 + (Ph1 + p_D D)^2}, \text{ and} \qquad \text{(A11)}$$

$$\text{grazing2} = r_C\frac{(Ph2 + Zo1)^2}{k_Z^2 + (Ph2 + Zo1)^2}. \qquad \text{(A12)}$$

Time-dependent temperature dependence is implemented according to the Q_{10} factors as defined in eq. (1): n_m and m_{pd} for phytoplankton; r_m, m_{zn} and m_{zd} for microzooplankton; and r_e, the remineralization rate representing indirectly the action of bacteria. The maximum *Zo2* grazing

rate r_C varies with temperature according to the same Q_{10} factor as for *Zo1*. The parameter m_{cn} represents the fraction of the food input to the mesozooplankton *Zo2* that is immediately excreted and converted back to the dissolved nutrient pool *N*. The remaining fraction is assumed over the course of a year to exit from the bottom of the model to the ocean interior, either as fecal pellets, unassimilated food, or as sinking or downward migrating mesozooplankton. This amount is added to the sinking flux of detritus *D* at the bottom of the model (120 m) to form the total annual loss to the ocean interior (*S* in Table 2) .

Acknowledgements

We thank PICES and the JGOFS North Pacific Task Team for organizing stimulating meetings and workshops where we received much constructive advice on earlier versions of this work. W.K. Li provided helpful advice and information on the the temperature dependence of bacterial production, and two referees, Mike Fasham and Fei Chai, provided helpful and constructive reviews. The long term monthly average wind speeds used to construct daily wind stress values were obtained on line from the US NOAA Live Access Server at the Pacific Marine Environmental Laboratory in Seattle.

References

Armstrong, R.A., 1994. Grazing limitation and nutrient limitation in marine ecosystems: steady state solutions of an ecosystem model with multiple food chains, Limnol. Oceanogr., 39, 597-608.

Banse, K., 1995. Zooplankton: Pivotal role in the control of ocean production, ICES Journal of Marine Science, 52, 265-277.

Boyd, P.W and P.J. Harrison, 1999. Phytoplankton dynamics in the NE subarctic Pacific, Deep-Sea Research II, 46, 2405-2432.

Boyd, P., A. Watson, C. Law, E. Abraham, T. Trull, R. Murdoch, D. Bakker, A. Bowle, K. Buesseler, H. Chang, M. Charette, P. Croot, K. Downing, R. Frew, M. Gall, M. Hadfield, J. Hall, M. Harvey, G. Jameson, J. LaRoche, M. Liddicoat, R. Ling, M. Maldonado, M. McKay, S. Nodder, S. Pickmere, R. Pridmore, S. Rintoul, K. Safi, P. Sutton, R. Strzepek, K. Tanneberger, S. Turner, A. Waite, and J. Zeldis, 2000. A mesoscale phytoplankton bloom in the polar Southern Ocean stimulated by iron fertilization, Nature, 407, 695-702.

Cavender-Bares, K.K., E.L. Mann, S.W. Chisholm, M.E. Ondrusek, and R.R. Bidigare, 1999. Differential response of equatorial Pacific phytoplankton to iron fertilization, Limnology and Oceanography, 44, 237-246.

Chai, R., R.C. Dugdale, T-H Peng, F.P. Wilkerson, and R.T. Barber, One dimensional ecosystem model of the equatorial Pacific upwelling system, Part I: Model development and silicon and nitrogen cycle, Deep-Sea Research II, in press.

Chisholm, S.W., 1992. Phytoplankton size, In: Primary Productivity and Biogeochemical Cycles in the Sea, P.G. Falkowski and A.D. Woodhead (eds.), Plenum, New York, pp. 213-237.

Coale, K.H., K.S. Johnson, S.E. Fitzwater, R.M. Gordon, S. Tanner, F.P. Chavez, L. Ferioli, C.

Sakamoto, P. Rogers, F. Millero, P. Steinberg, P. Nightingale, D. Cooper, W.P. Cochlan, M.R. Landry, J. Constantinou, G. Rollwagen, A. Trasvina, and R. Kudela, 1996. A massive phytoplankton bloom induced by an ecosystem-scale iron fertilization experiment in the equatorial Pacific Ocean, Nature, 383, 495-501.

Cox, P.M., R.A. Betts, C.D. Jones, S.A. Spall, and I.J. Totterdell, 2000. Acceleration of global warming due to carbon-cycle feedbacks in a coupled climate model, Nature, 408, 184-187.

Denman, K.L., and M.A. Peña, 1999. A coupled 1-D biological / physical model of the northeast subarctic Pacific Ocean with iron limitation, Deep-Sea Research II, 46, 2877-2908.

Denman, K.L., M.A. Peña, and S.P. Haigh, 1998. Simulations of marine ecosystem response to climate variation with a one dimensional coupled ecosystem/mixed layer model, pp. 141-147, In: G. Holloway, P. Müller, and D. Henderson (eds.), Biotic Impacts of Extratropical Climate Variability in the Pacific, Proceedings 1998 'Aha Huliko'a Hawaiian Winter Workshop, University of Hawaii at Manoa.

Doney, S.C., 1999. Major challenges confronting marine biogeochemical modeling, Global Biogeochemical Cycles, 13, 705-714.

Edwards, A.M., and A. Yool, 2000. The role of higher predation in plankton population models, Journal of Plankton Research, 22, 1085-1112.

Eppley, R.W., 1972: Temperature and phytoplankton growth in the sea, Fishery Bulletin, 70, 1063-1085.

Fasham, M.J.R., 1993. Modelling the marine biota, pp. 457-504, In: The Global Carbon Cycle, M. Heimann (ed.), Springer-Verlag, Berlin.

Fasham, M.J.R., P.W. Boyd, and G. Savidge, 1999. Modeling the relative contributions of autotrophs and heterotrophs to carbon flow at a Lagrangian JGOFS station in the Northeast Atlantic: The importance of DOC, Limnology and Oceanography, 44, 80-94.

Fasham, M.J., and G.T. Evans, 1995. The use of optimization techniques to model marine ecosystem dynamics at the JGOFS station at 47° N 20° W, Phil. Trans. R. Soc. Lond. B, 348, 203-209.

Fasham, M.J.R., J.L. Sarmiento, R.D. Slater, H.W. Ducklow, and R. Williams, 1993. Ecosystem behavior at Bermuda Station "S" and Ocean Weather Station "India": a general circulation model and observational analysis, Global Biogeochem. Cycles, 7, 379-415.

Freeland, H.J., K.L. Denman, C.S. Wong, F. Whitney, and R. Jacques, 1997. Evidence of change in the winter mixed layer in the northeast Pacific Ocean, Deep-Sea Research I, 44, 2117-2129.

Fulton, J.D., 1983. Seasonal and annual variation in net zooplankton at Ocean Station P, 1956-1980, Canadian Data Report of Fisheries and Aquatic Sciences, 374, 65pp.

Fung, I.Y., S.K. Meyn, I. Tegen, S.C. Doney, J.G. John, and J.K. Bishop, 2000. Iron supply and demand in the upper ocean, Global Biogeochemical Cycles, 14, 281-295.

Gargett, A.E., 1991. Physical processes and the maintenance of nutrient-rich euphotic zones, Limnology and Oceanography, 36, 1527-1545.

Goldblatt, R.H., D.L. Mackas and A.G. Lewis, 1999. Mesozooplankton community characteristics in the NE subarctic Pacific, Deep-Sea Research II, 46, 2619-2644.

Haigh, S.P., K.L. Denman, and W.W. Hsieh, 2001. Simulation of the planktonic ecosystem response to pre- and post-1976 forcing in an isopycnic model of the North Pacific, Canadian Journal of Fisheries and Aquatic Sciences, 58, 703-722.

Harrison, P.J., P.W. Boyd, D.E. Varela, S. Takeda, A. Shiomoto and T. Odate, 1999. Comparison of factors controlling phytoplankton productivity in the NE and NW subarctic Pacific gyres, Progress in Oceanography, 43, 205-234.

Huntley, M.E., and M.D. Lopez, 1992. Temperature-dependent production of marine copepods: a global synthesis, The American Naturalist, 140, 201-242.

IPCC, 2001. Intergovernmental Panel on Climate Change, Working Group I, Third Assessment Report, in press.

Joint, I., A. Pomroy, G. Savidge, and Philip Boyd, 1993. Size-fractionated primary productivity in the northeast Atlantic in May-July 1989. Deep-Sea Research II, 40, 423-440.

Kawamiya, M., M.J. Kishi, Y. Yamanaka, and N. Suginohara, 1995. An ecological-physical coupled model applied to Station Papa, Journal of Oceanography, 51, 635-664.

Kirchman, D.L., R.G. Keil, M. Simon, and N.A. Welschmeyer, 1993. Biomass and production of heterotrophic bacterioplankton in the oceanic subarctic Pacific, Deep-Sea Research I, 40, 967-988.

Kirchman, D.L., and J.H. Rich, 1997. Regulation of bacterial growth rates by dissolved organic carbon and temperature in the equatorial Pacific Ocean, Microbial Ecology, 33, 11-20.

Laws, E.A., P.G. Falkowski, W.O. Smith, Jr., H. Ducklow, and J.J. McCarthy, 2000. Temperature effects on export production in the open ocean, Global Biogeochemical Cycles, 14, 1231-1246.

Leonard, C.L., C.R. McClain, R. Murtugudde, E.E. Hofmann, and L.W. Harding, Jr., 1999. An iron-based ecosystem model of the central equatorial Pacific, Journal of Geophysical Research, 104, 1325-1341.

Li., W.K., 1998. Annual average abundance of heterotrophic bacteria and *Synechococcus* in surface ocean waters, Limnology and Oceanography, 43, 1746-1753.

Loukos, H., B. Frost, D.E. Harrison, and J.W. Murray, 1997. An ecosystem model with iron limitation of primary production in the equatorial Pacific at 140°W, Deep-Sea Research II, 44, 2221-2249.

McClain, C.R., K. Arrigo, K.-S. Tai, and D. Turk, 1996. Observations and simulations of physical and biological processes at ocean weather station P, 1951-1980. Journal of Geophysical Research, 101, 3697-3713.

Mann, E.L., and S.W. Chisholm, 2000. Iron limits the cell division rate of *Prochlorococcus* in the eastern equatorial Pacific, Limnology and Oceanography, 45, 1067-1076.

Martin, J.H., 1990. Glacial-interglacial CO_2 change: the iron hypothesis, Palaeoceanography, 5, 1-13.

Matear, R.J., 1995. Parameter optimization and analysis of ecosystem models using simulated annealing: A case study at Station P, J. Mar. Res., 53, 571-607.

Mellor, G.L., and T. Yamada, 1982. Development of a turbulent closure model for geophysical fluid problems, Rev. Geophys. Space Phys., 20, 851-875.

Oschlies, A., and V. Garçon, 1999. An eddy-permitting coupled physical-biological model of the North Atlantic. 1. Sensitivity to advection numerics and mixed layer physics, Global Biogeochemical Cycles, 13, 135-160.

Polovina, J.J., G.T. Mitchum, and G.T. Evans, 1995. Decadal and basin-scale variation in mixed layer depth and the impact on biological production in the Central and North Pacific, 1960-88, Deep-Sea Research I, 42, 1701-1716.

Pondaven, P., D. Ruiz-Pino, J.N. Druon, C. Fravalo, and P. Trenguer, 1999. Factors controlling silicon and nitrogen biogeochemical cycles in high nutrient, low chlorophyll systems (the Southern Ocean and the North Pacific): Comparison with a mesotrophic system (the North Atlantic), Deep-Sea Research, 46, 1923-1968.

Raimbault, P. M. Rodier, and I. Taupier-Letage, 1988. Size fraction of phytoplankton in the Ligurian Sea and the Algerian Basin (Mediterranean Sea): Size distribution versus total concentration, Marine Microbial Food Webs, 3, 1-7.

Rivkin, R.B., J.N. Putland, M.R. Anderson and D. Deibel, 1999. Microzooplankton bacterivory and herbivory in the NE subarctic Pacific, Deep-Sea Research II, 46, 2579-2618.

Sarmiento, J.L., T.M.C. Hughes, R.J. Stouffer, S. Manabe, R.J. Stouffer, 1998. Simulated response of the ocean carbon cycle to anthropogenic climate warming, Nature, 393, 245-249.

Sarmiento, J.L., R.D. Slater, M.J.R. Fasham, H.W. Ducklow, J.R. Toggweiler, and G.T. Evans, 1993. A seasonal three-dimensional ecosystem model of nitrogen cycling in the North Atlantic euphotic zone, Global Biogeochem. Cycles, 7, 379-415.

Savidge, G., P. Boyd, A. Pomroy, D. Harbour, and I. Joint, 1995. Phytoplankton production and biomass estimates in the northeast Atlantic Ocean, May-June 1990, Deep-Sea Research I, 42, 599-617.

Shiomoto, A., K. Tadokoro, K. Monaka, and M. Nanba, 1997. Productivity of picoplankton compared with that of larger phytoplankton in the subarctic region, Journal of Plankton Research, 19, 907-916.

Søndergaard, M., L.M. Jensen, and G. Aertebjerg, 1991. Picoalgae in Danish coastal waters during summer stratification, Marine Ecology Progress Series, 79, 139-149.

Vézina, A.F. and T. Platt, 1988. Food web dynamics in the ocean. I. Best-estimates of flow networks using inverse methods. Mar. Ecol. Prog. Ser., 42: 269-287.

White, P.A., J. Kalff, J.B. Rasmussen, and J.M. Gasol, 1991. The effect of temperature and algal biomass on bacterial production and specific growth rate in freshwater and marine habitats, Microbial Ecology, 21, 99-118.

Whitney, F.A., and H.J. Freeland, 1999. Variability in upper-ocean water properties in the NE Pacific Ocean, Deep-Sea Research II, 46, 2351-2370.

Table 1. Model parameters for OSP simulations for Mark 1 model and enhanced Mark 2 model.

Parameter	**Symbol**	**Units**	**Mark 1**	**Mark 2**
PAR attenuation coefficient for sea water	k_w	m^{-1}	0.04	0.04
PAR attenuation coefficient for (*P+D*)	k_c	m^{-1} (mmol-N m^{-3})$^{-1}$	0.06	0.06
Initial slope of P-I curve	a	d^{-1} (W m^{-2})$^{-1}$ #	0.08	0.08
Maximum phytoplankton growth rate	v_m	d^{-1}	2.0	1.5*
Nutrient half saturation constant	k_n	mmol-N m^{-3}	0.1	0.1
Phytoplankton mortality rate (to Detritus)	m_{pd}	d^{-1}	0.05	0.05
Microzooplankton maximum grazing rate	r_m	d^{-1}	1.0	1.0
Microzooplankton assimilation efficiency	g_a	-	0.7	0.7
Microzooplankton grazing half saturation constant	k_P	mmol-N m^{-3}	0.4	0.75*
Microzooplankton losses to Nutrients	m_{zn}	d^{-1}	0.20	0.03*
Microzooplankton losses to Detritus	m_{zd}	d^{-1}	0.05	-*
Detritus sinking speed	w_s	m d^{-1}	6	6
Detritus remineralization rate	r_e	d^{-1}	0.1	0.1
Maximum concentration of small phytoplankton *Ph1*	P_S	mmol-N m^{-3}	-	2.0
Phytoplankton concentration when $Ph1 = 0.5P_S$	k_S	mmol-N m^{-3}	-	2.5
Microzooplankton relative preference for Detritus	p_D	-	-	0.5
Mesozooplankton maximum grazing rate	r_C	d^{-1}	-	0.5
Mesozooplankton grazing half saturation constant	k_Z	mmol-N m^{-3}	-	0.6
Mesozooplankton excretion factor	m_{cn}	-	-	0.3
Iron limitation value	L_{Fe}	-	0.35, 1.0	0.3*, 1.0

$d^{-1} \equiv day^{-1}$

* changed from Mark 1 simulations

Table 2. Comparison of major fluxes between the different simulations: PP = Primary production (mol-N m^{-2} y^{-1}), DN = winter to summer drawdown of mixed layer nutrient (mmol-N m^{-3}), $Zo2_L$ = Zo2 losses after excretion (mol-N m^{-2} y^{-1}), S = (sinking flux of D at 120m + $Zo2_L$) in (mol-N m^{-2} y^{-1}), and ER = Export ratio.

Run	**Model**	**PP**	DN	S	**$Zo2_L$**	**ER = S / PP**	**$\frac{Zo2_L}{PP}$**
1	Mark 1 Standard	1.36	7.6	0.30	—	0.22	—
2	ΔT = 2°C	1.51	8.1	0.26	—	0.17	—
3	No Fe limitation	2.26	13.6	0.38	—	0.17	—
4	Mark 2 Standard	0.88	7.5	0.38	0.23	0.43	0.26
5	ΔT = 2°C	0.98	8.2	0.39	0.26	0.40	0.26
6	ΔT = 5°C	1.16	9.5	0.40	0.30	0.34	0.26
7	No Fe limitation	1.65	10.5	0.52	0.37	0.31	0.22

Figure Captions

Figure 1. Annual fluxes integrated over the layer 0-50 m for the Mark 1 model for the iron limited case (in units of mol-N m^{-2} y^{-1}). This case corresponds to the standard run in Denman and Peña, 1999) but now including temperature dependence of physiological rates. Double-ended arrows represent mixing fluxes between the top 50-m layer and below (+ve upwards), much of the flux resulting from entrainment/detrainment associated with the annual cycle in the mixed layer thickness. The downward arrow from *D* represents particles sinking past the 50-m and 120-m levels. The upward arrow labelled f_{up} represents 'upwelled' nutrient injected over the bottom 5 grid layers.

Figure 2. Results of the the Mark 1 model simulations removing iron limitation and increasing the temperature by 2°C (in parentheses). Only fluxes and pool sizes that changed by at least 15% are shown. Percent changes in mixed layer pool sizes (*Z* and *D*) are for the time of summer maximum in zooplankton *Z*: those mixed layer concentrations in the 'reference' run of Fig. 1 for *P*, *Z* and *D* are 0.30, 0.33 and 0.16 (all in mol-N m^{-2} y^{-1}). The %-change in 'ΔN' represents the %-change in the drawdown in surface nitrate from the winter maximum to the summer minimum concentration. Mixing rates (double-ended arrows) do not change sign/direction from Figure 1.

Figure 3. Biomass of the small (<5 μm) fraction of the phytoplankton plotted against the total concentration of phytoplankton: (a) for a variety of sources in the N. Atlantic and N. Pacific, and (b) for observations from the vicinity of OSP in the subarctic N. Pacific. The curve is eq. (2), used to partition the phytoplankton into a small fraction *Ph1* and a large fraction *Ph2*, with P_S=2 and k_S =2.5, both in units of (mmol-N m^{-3}), taken to be equal to (mg-Chl m^{-3}).

Figure 4. Schematic of the Mark 2 enhanced ecosystem model. Phytoplankton are partitioned into small *Ph1* (<5 μm) and large *Ph2* (>5 μm) cells according to the total biomass. Imposed meso-

zooplankton grazing follows the average seasonal cycle from long term observations at Ocean Station P (lower right panel). Dashed lines represent additional fluxes in the enhanced ecosystem model. Annual fluxes (in mol-N m^{-2}) for the iron-limited case as in Figure 1.

Figure 5. Time-depth plots for the Mark 2 iron limited simulation of Figure 4. Top panel: contours of constant temperature. Dotted line represents represents maximum daily diagnosed mixed layer depth, red dot-dashed line represents minimum daily mixed layer depth, and dashed line represents 1% I_{PAR} penetration depth. Second panel: lines represent averages of *N*, *P*, *Zo1* and *D* over the depth range 0-50 m; and bottom two panels: *P* and *D* contours (all in units of mmol-N m^{-3}).

Figure 6. Mark 2 model %-changes (≥ 15%) from Figure 4 in *maximum* mixed layer pool sizes and annual average fluxes (0-50m) for climate change simulations: (a) 2°C (in parentheses) and 5°C warming offsets, and (b) removal of iron limitation on phytoplankton production. The 'reference' run (Fig. 4) maximum mixed layer concentrations for *P*, *Zo1* and *D* are 0.51, 0.91 and 0.13 (all in mol-N m^{-3}). As in Figure 2, 'ΔN' represents the %-change in the drawdown in surface nitrate from the winter maximum to the summer minimum concentration.

Figure 7. Time-depth contour plots of microzooplankton *Zo1* for the Mark 2 simulations: Upper panel: iron limited simulation (corresponding to Figs. 4 and 5); and lower panel: simulation with removal of iron limitation.

Figure 8. Sensitivity of Mark 2 model to changes in Q_{10} values over a range of a factor of 10 for 2°C warming simulation, normalized to the values of Run 5 (parameter values referenced to 10°C): (a) relative changes in annual primary production *PP* and annual export ratio *ER* = *S*/*PP*; (b) relative changes for varying Q_{10}(zooplankton) while keeping the other Q_{10} values constant; and (c) relative changes for varying Q_{10}(bacteria) while keeping the other Q_{10} values constant.

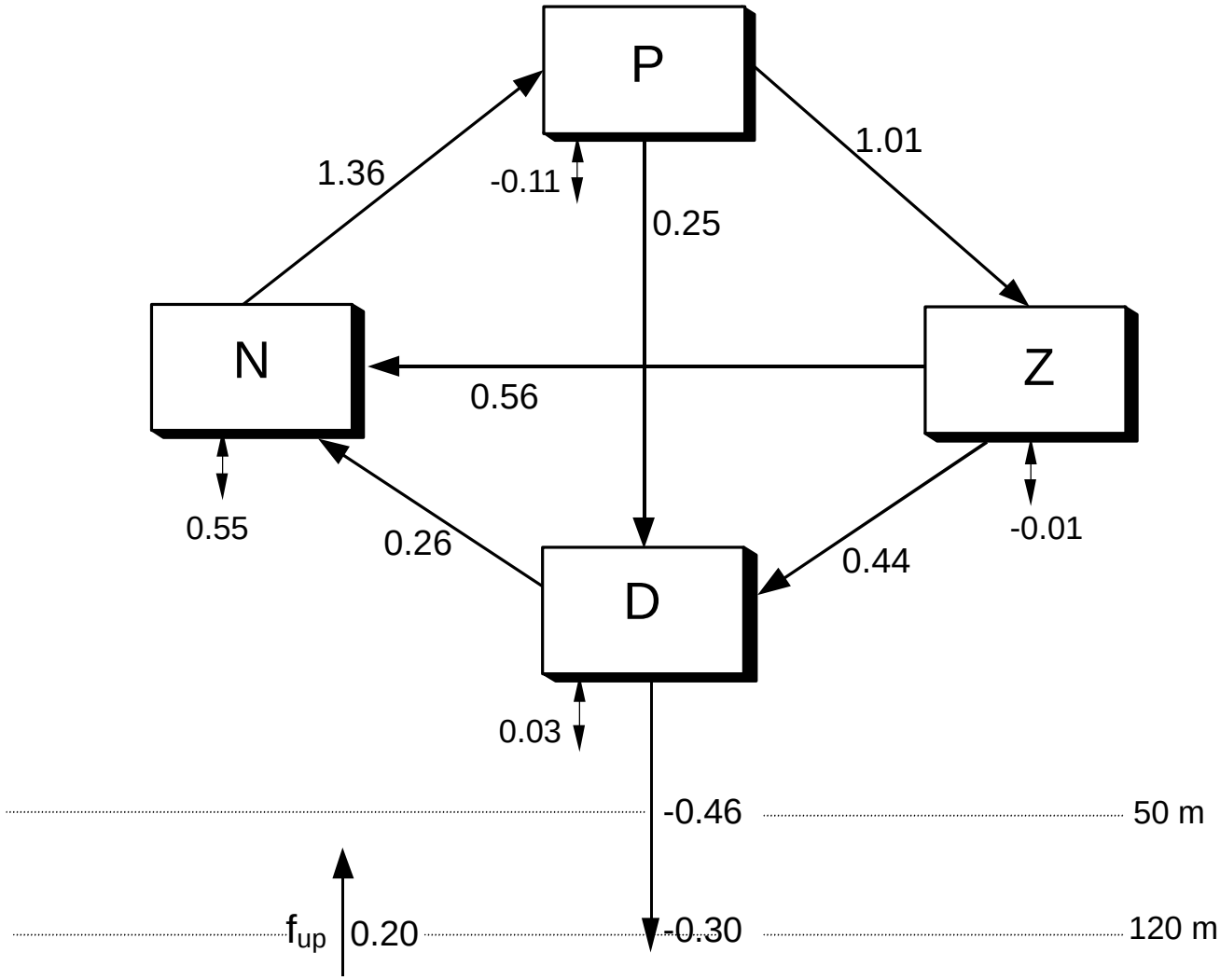
P
N
Z
D
1.36
-0.11
0.25
1.01
0.56
0.55
0.26
0.44
-0.01
0.03
-0.46
50 m
f_{up}
0.20
-0.30
120 m

Fig. 1

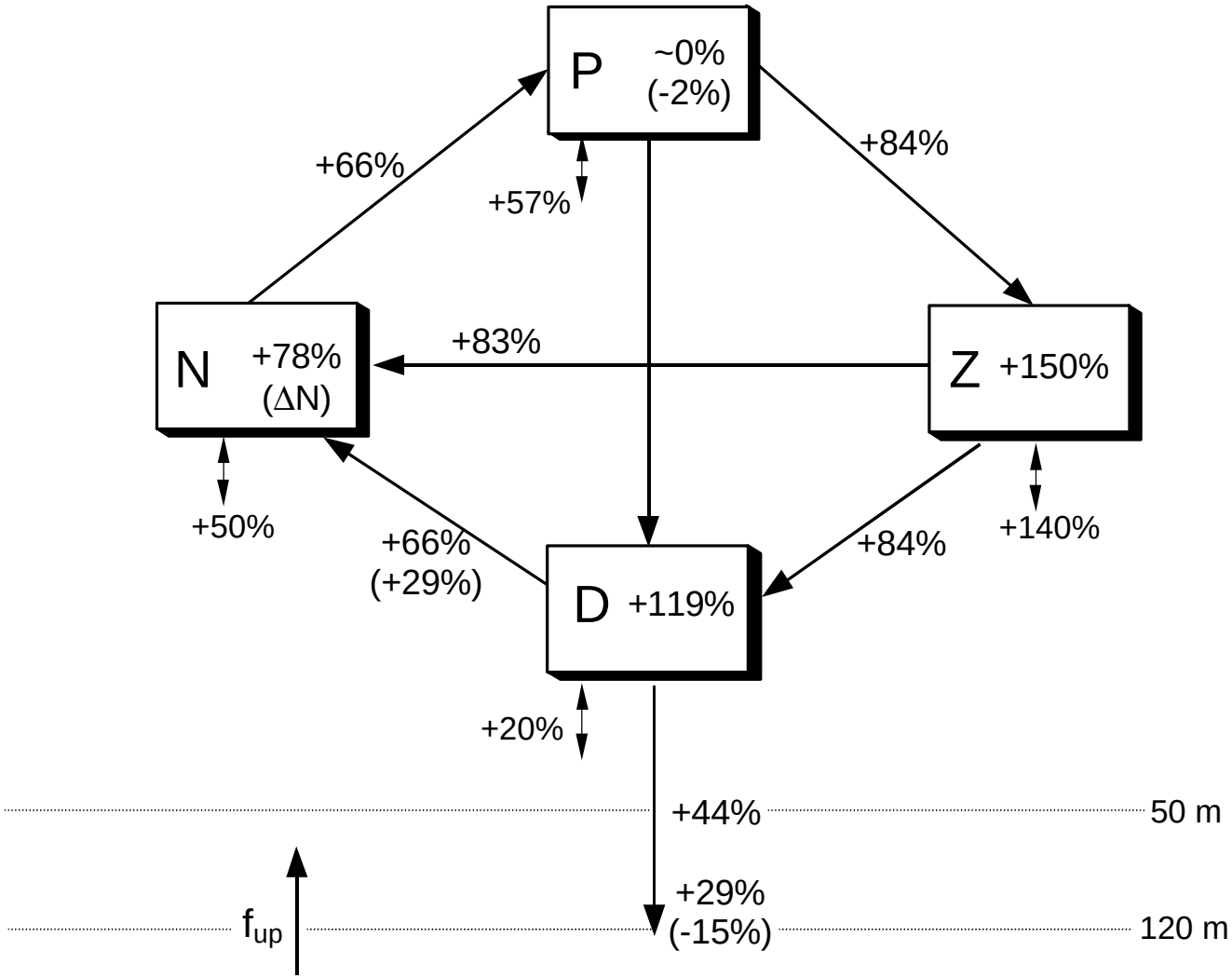
P
~0%
(-2%)
+66%
+57%
+84%
N
+78%
(ΔN)
+83%
Z
+150%
+50%
+66%
(+29%)
+84%
+140%
D
+119%
+20%
+44%
50 m
+29%
(-15%)
f up
120 m

Fig. 2

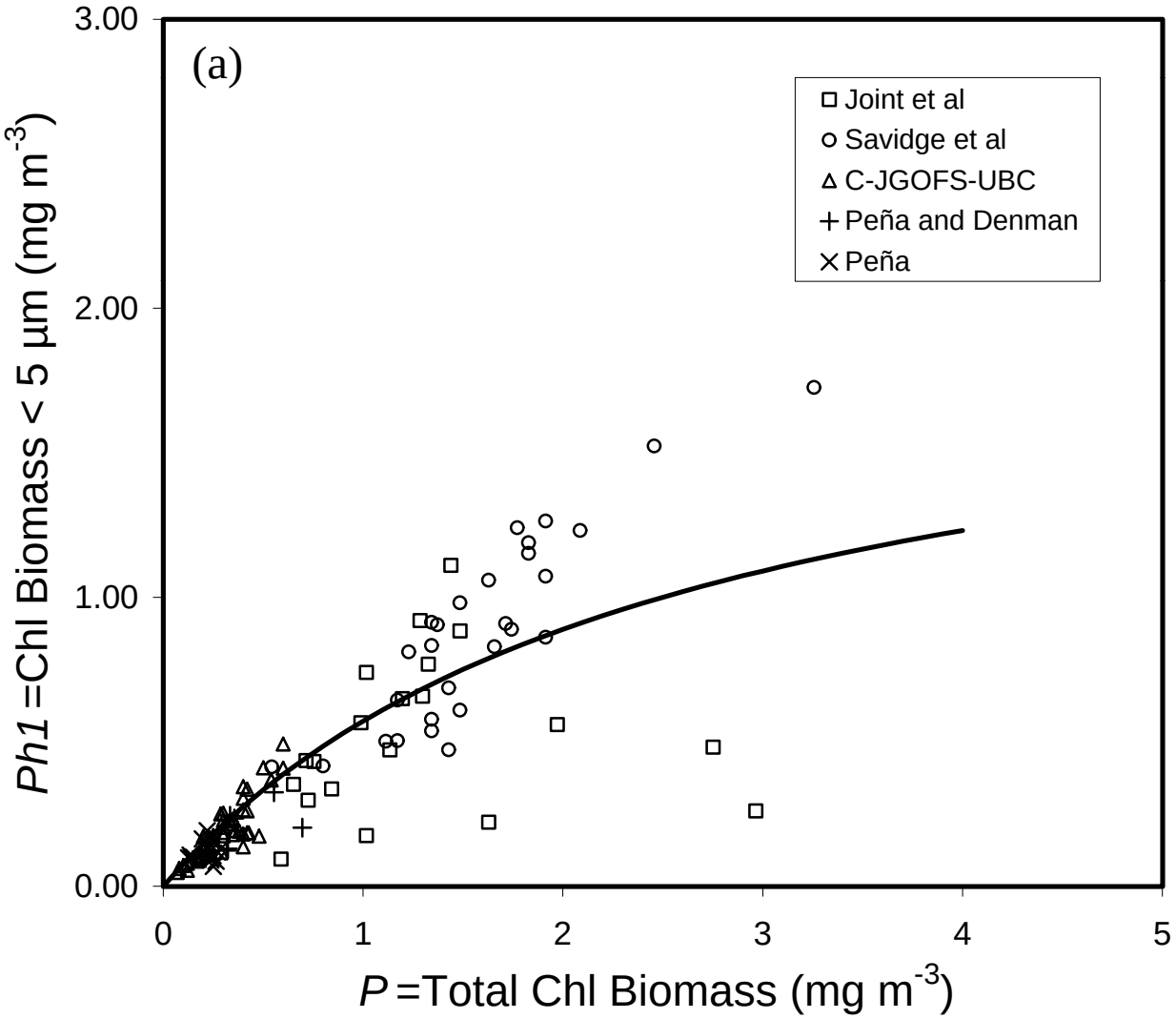
(a)
Joint et al
Savidge et al
C-JGOFS-UBC
Peña and Denman
Peña
3.00
2.00
1.00
0.00
0
1
2
3
4
5
Ph1 =Chl Biomass < 5 µm (mg m-3)
P =Total Chl Biomass (mg m-3)

Fig. 3a

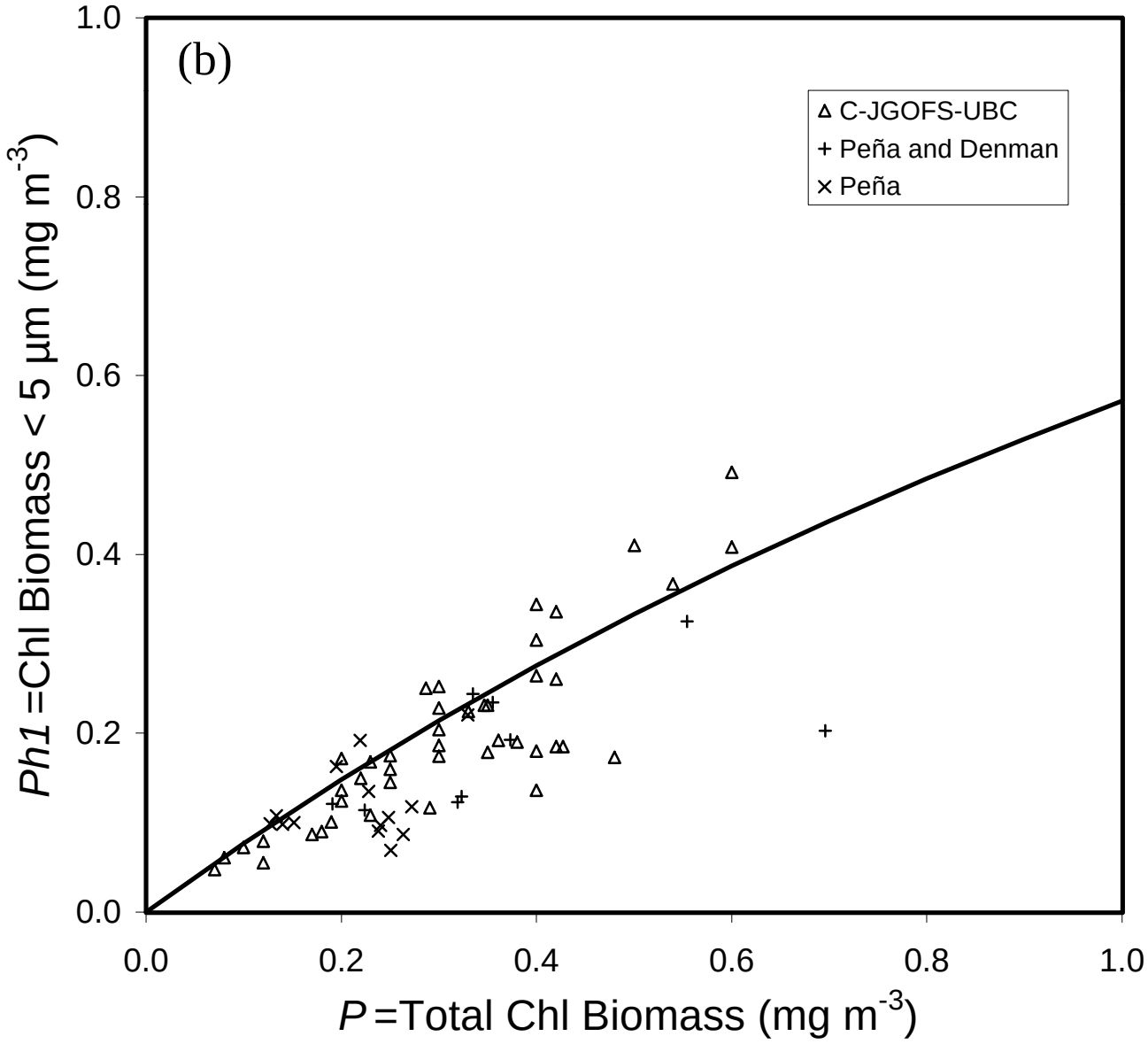
(b)
C-JGOFS-UBC
Peña and Denman
Peña
1.0
0.8
0.6
0.4
0.2
0.0
0.0
0.2
0.4
0.6
0.8
1.0
Ph1 =Chl Biomass < 5 µm (mg m-3)
P =Total Chl Biomass (mg m-3)

Fig. 3b

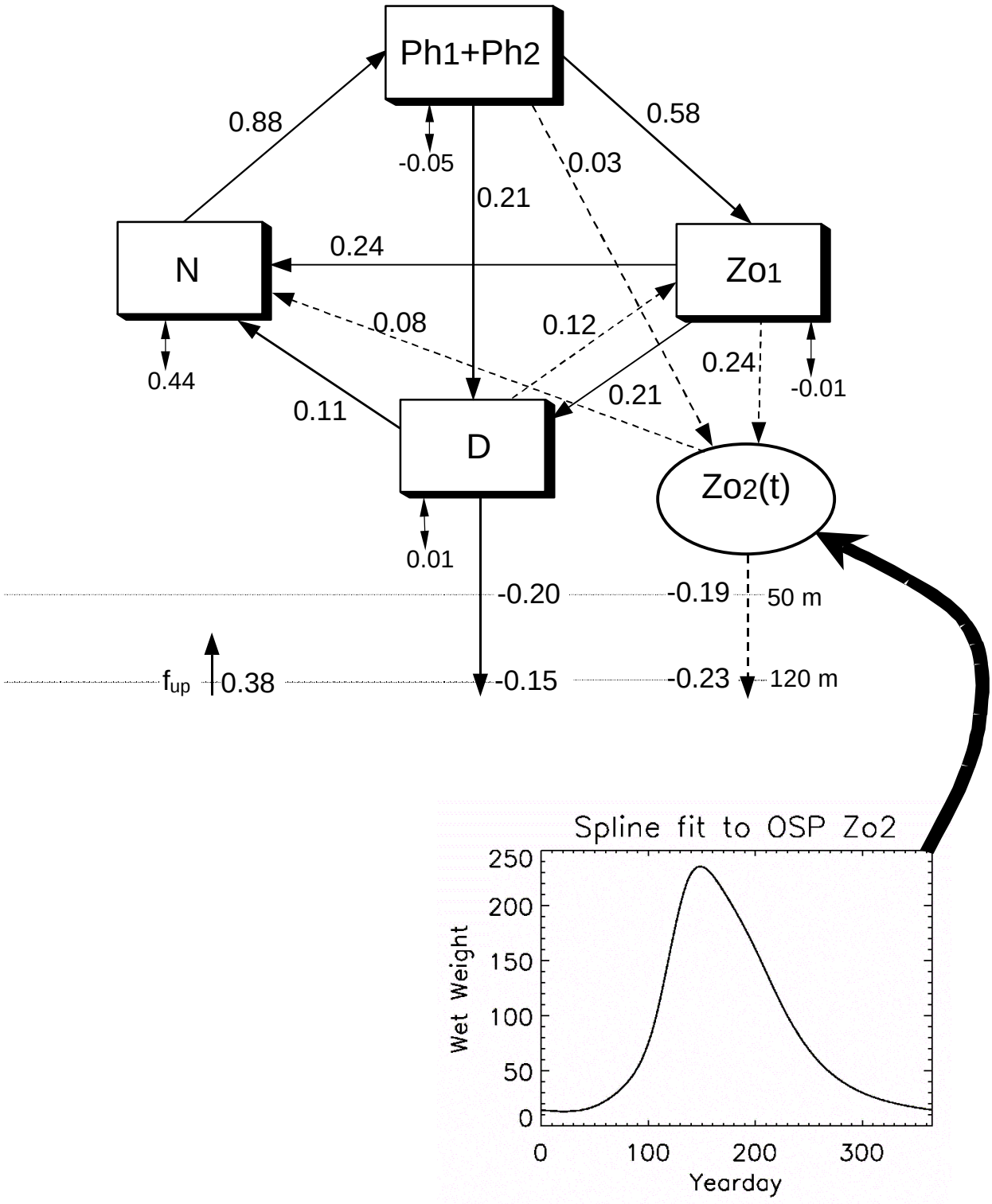
Ph1+Ph2
0.88
0.58
-0.05
0.03
0.21
N
0.24
Zo1
0.08
0.12
0.44
0.24
-0.01
0.11
0.21
D
Zo2(t)
0.01
-0.20
-0.19
50 m
fup
0.38
-0.15
-0.23
120 m
Spline fit to OSP Zo2
Wet Weight
250
200
150
100
50
0
0
100
200
300
Yearday

Fig. 4

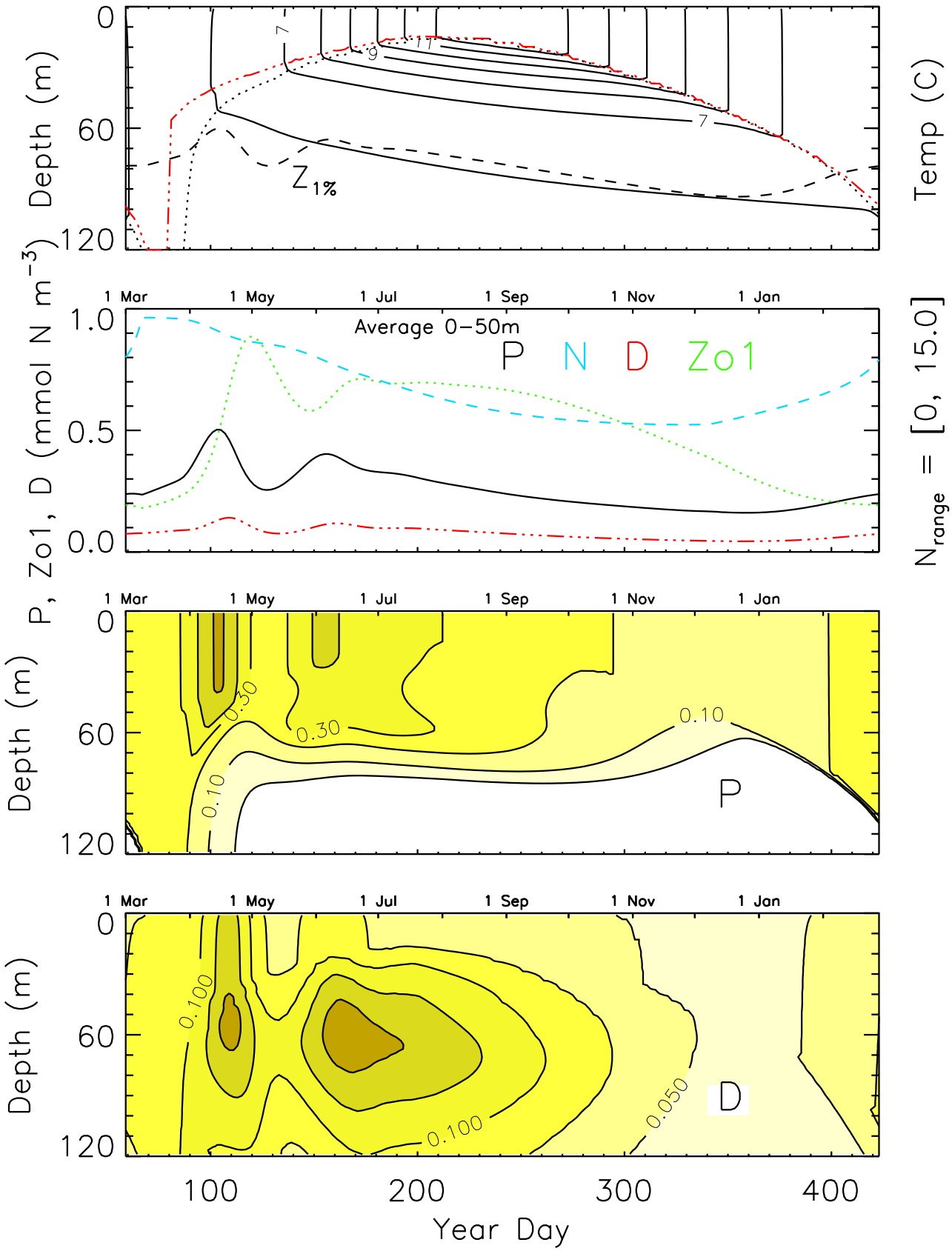
Depth (m)
0
60
120
7
9
11
7
$Z_{1\%}$
Temp (C)
1 Mar
1 May
1 Jul
1 Sep
1 Nov
1 Jan
P, Zo1, D (mmol N m^{-3})
1.0
0.5
0.0
Average 0–50m
P N D Zo1
N_{range} = [0, 15.0]
Depth (m)
0.30
0.30
0.10
0.10
P
0.100
0.100
0.050
D
100
200
300
400
Year Day

Fig. 5

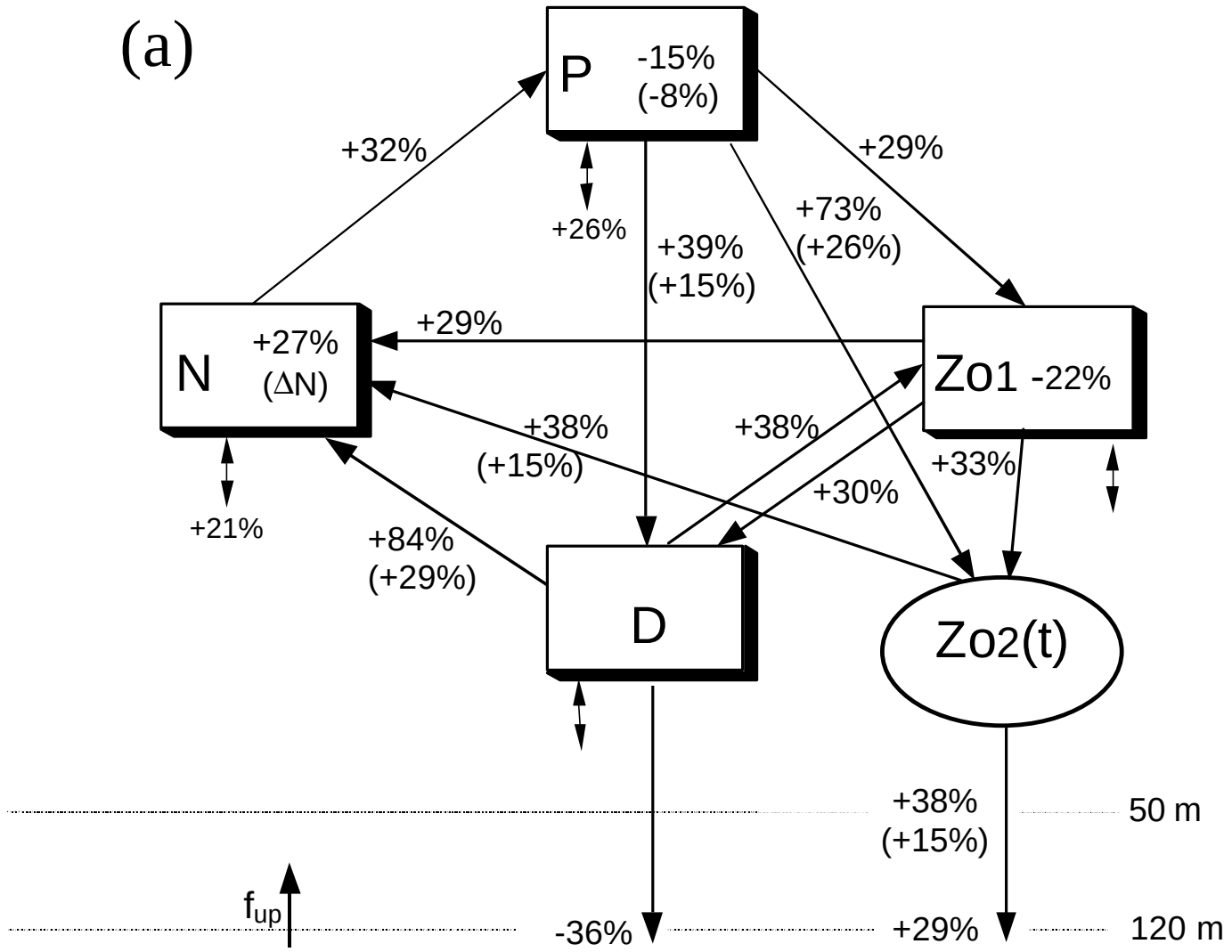
(a)
P
-15%
(-8%)
+32%
+26%
+39%
(+15%)
+73%
(+26%)
+29%
N
+27%
(ΔN)
+29%
Zo1 -22%
+38%
(+15%)
+38%
+30%
+33%
+21%
+84%
(+29%)
D
Zo2(t)
+38%
(+15%)
50 m
fup
-36%
+29%
120 m

Fig. 6a

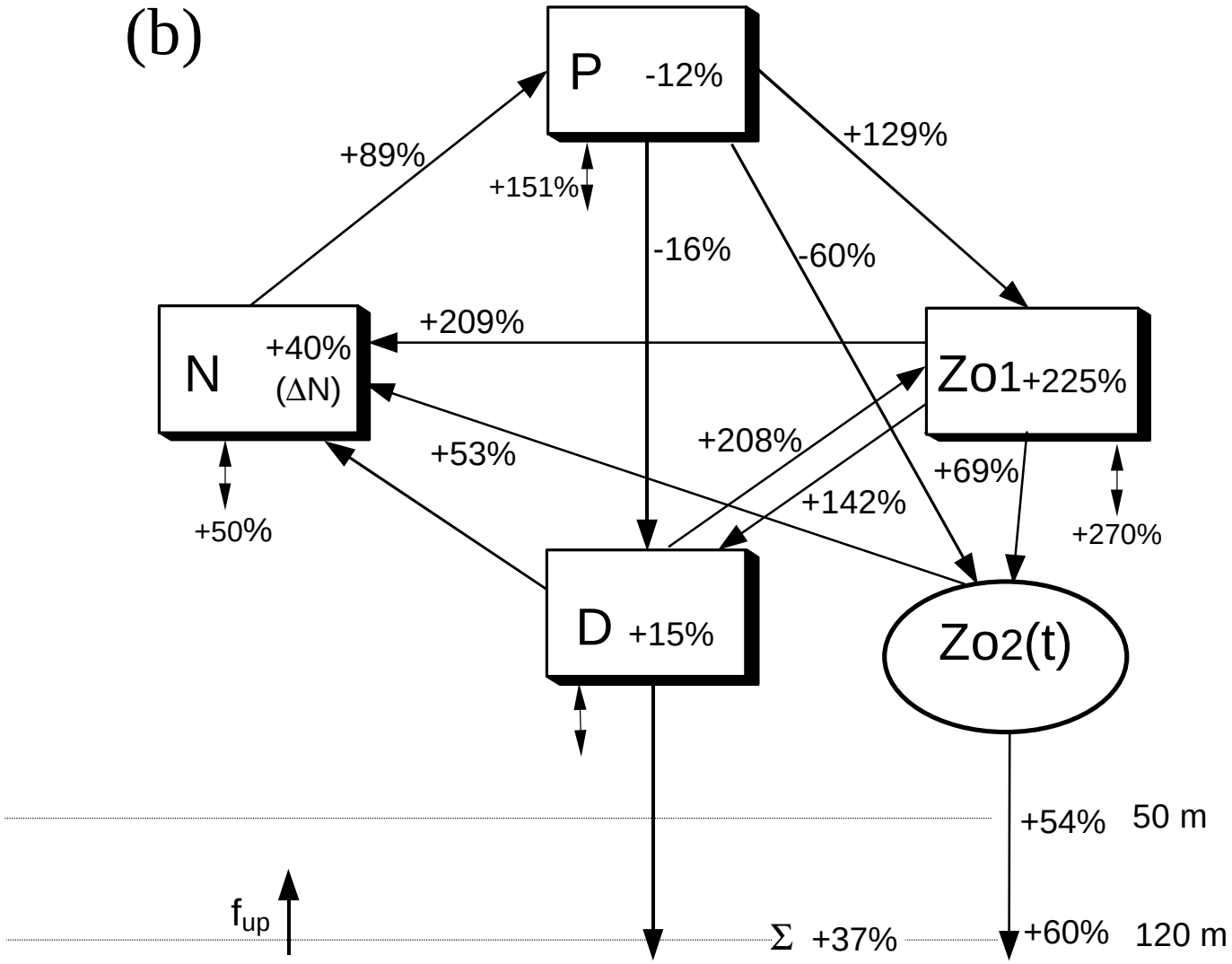
(b)
P -12%
+89%
+151%
+129%
-16%
-60%
N +40% (ΔN)
+209%
Zo1+225%
+208%
+53%
+69%
+142%
+50%
+270%
D +15%
Zo2(t)
+54% 50 m
fup
Σ +37%
+60% 120 m

Fig. 6b

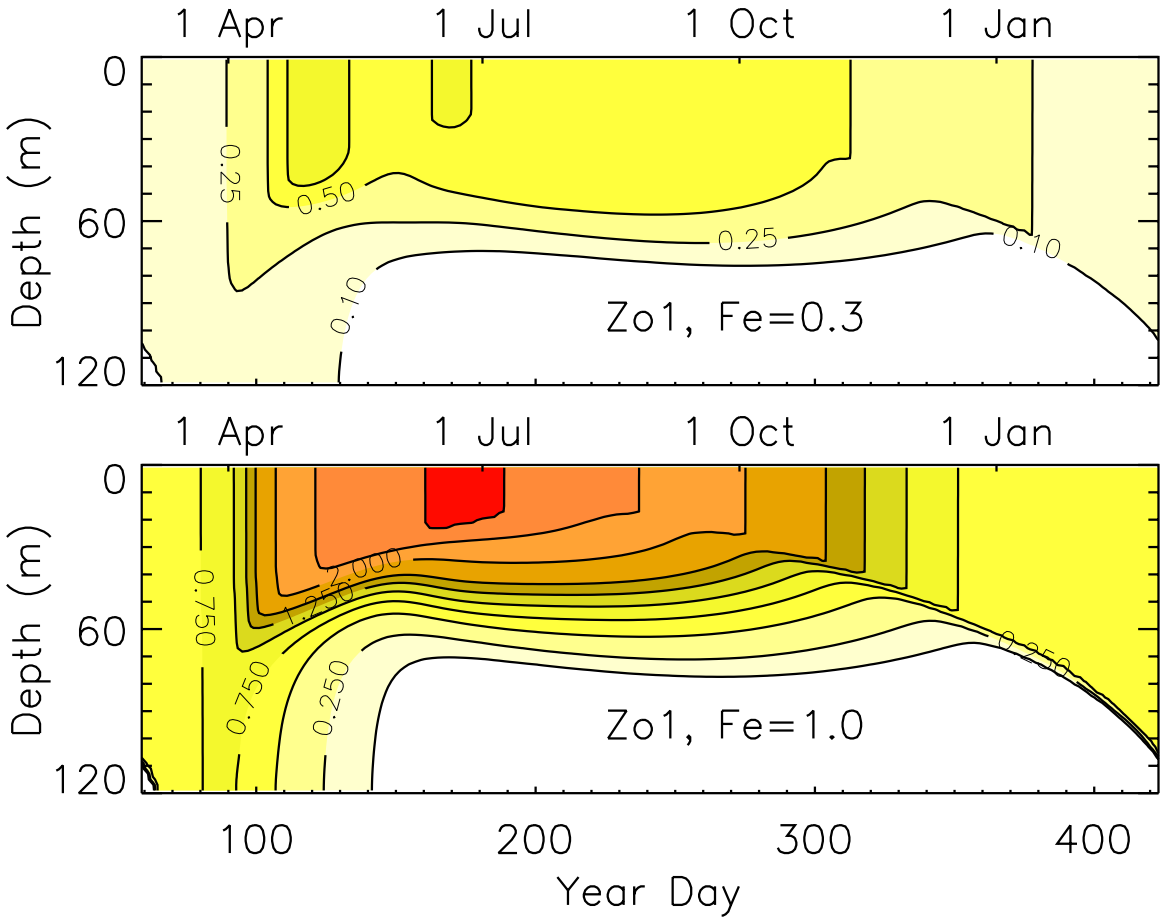
1 Apr
1 Jul
1 Oct
1 Jan
Depth (m)
0
60
120
0.25
0.50
0.25
0.10
0.10
Zo1, Fe=0.3
1 Apr
1 Jul
1 Oct
1 Jan
Depth (m)
0
60
120
0.750
2.000
1.750
0.750
0.250
0.250
Zo1, Fe=1.0
100
200
300
400
Year Day

Fig. 7

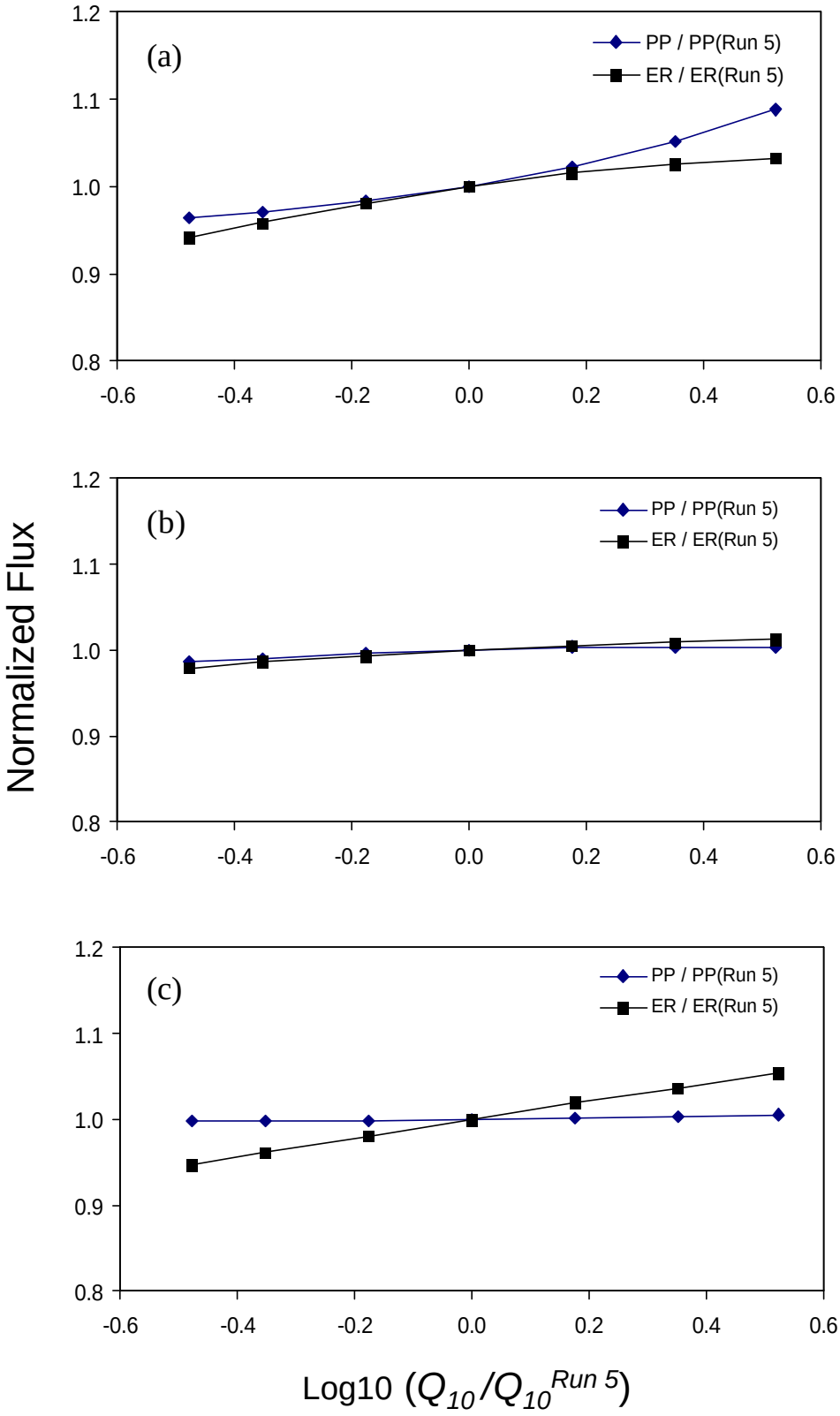
(a)
PP / PP(Run 5)
ER / ER(Run 5)
(b)
PP / PP(Run 5)
ER / ER(Run 5)
(c)
PP / PP(Run 5)
ER / ER(Run 5)
Normalized Flux
Log10 ($Q_{10}/Q_{10}^{Run\ 5}$)
1.2
1.1
1.0
0.9
0.8
-0.6
-0.4
-0.2
0.0
0.2
0.4
0.6

Fig. 8